Spectrochimica Acta Part A 77 (2010) 612–619

Contents lists available at ScienceDirect

Spectrochimica Acta Part A: Molecular and Biomolecular Spectroscopy

journal homepage: www.elsevier.com/locate/saa

Molecular structure, anharmonic vibrational frequencies and NBO analysis of naphthalene acetic acid by density functional theory calculations

E. Kavitha [a], N. Sundaraganesan [a,*], S. Sebastian [a], M. Kurt [b]

[a] Department of Physics (Engg.), Annamalai University, Annamalai Nagar, Chidambaram, Tamil Nadu 608 002, India
[b] Ahi Evran Őniversitesi Fen Edebiyat Fakőltesi Fizik Bölőmő, Asıkpasa Kampuső, 40100 Kirsehir-Turkiye, Turkey

ARTICLE INFO

Article history:
Received 11 April 2010
Received in revised form 30 May 2010
Accepted 18 June 2010

Keywords:
FT-IR
FT-Raman
Anharmonic frequencies
Dimer
NAA
DFT

ABSTRACT

In this work, we report anharmonic vibrational frequencies, molecular structure, NBO and HOMO, LUMO analysis of naphthalene acetic acid (NAA). The optimized geometric bond lengths and bond angles obtained by computation show good agreement with experimental X-ray data. The computed dimer parameters also show good agreement with experimental data. Anharmonic frequencies of NAA were determined and analyzed by DFT level of theory utilizing 6-311+G(d,p) basis set. Good agreement between the calculated and experimental spectra was obtained. Stability of the molecule arising from hyperconjugative interactions and charge delocalization have been analyzed using natural bond orbital (NBO) analysis. The results show that charge in electron density (ED) in the π^* and σ^* antibonding orbitals and E2 energies. This confirms the occurrence of ICT (Intermolecular Charge Transfer) within the molecule. The calculated HOMO and LUMO energies also show that charge transfer occurs within the molecule.

1. Introduction

Naphthalene acetic acid derivatives are non-steroidal anti-inflammatory drugs (NSAIDS) that exhibit favorable anti-inflammatory, analgesia and antipyretic properties. The major clinical application on NSAIDS is their action as anti-inflammatory agent in muscle skeletal disease [1]. 2-Acetonaphthalene provides the best raw materials, for the preparation of 2-naphthoic acid. It undergoes electrophilic aromatic substitution reaction. It is used as an intermediate for synthesis of pharmaceuticals, photochemicals, plant growth hormones, insecticides, dyes and other organic compounds. It is used in different pathways for the degradation of salicylic acid. Considerations of these factors leads to detailed spectral investigation of NAA.

Harmonic frequencies that are calculated on the basis of quantum mechanical force field usually differ from observed frequencies partly because of approximation in quantum mechanical methods and partly because of anharmonicity. Anharmonic treatment becomes important in biomolecular spectroscopy when dealing with complex molecular structures. With the development of quantum chemical procedures rooted in the framework of density functional theory (DFT) and Hatree–Fock (HF) theory, reliable anharmonic computations of vibrational frequencies for medium and large sized molecules in vacuum have become possible. The inclusion of anharmonic contribution reduces the absolute error. Many workers have performed theoretical anharmonic calculations on small and large molecules [2–4]. Structures and harmonic vibrational frequencies of 2-naphthoic acid and 6-bromo-2-naphthoic acid based on density functional theory calculations have been reported by Krishnakumar et al. [5]. In our earlier study, we reported the spectroscopic FT-IR gas phase, FT-Raman, hyperpolarizability analysis of napthhoic acid by ab initio HF and density functional methods [6]. Recently harmonic frequencies of 1-naphthyl acetic acid computed using B3LYP/6-311+G(d,p) method have been reported by Krishnakumar et al. [7]. In this work the detailed molecular structure was not compared with X-ray crystal data, and the earlier assignments of the spectra of NAA are still ambiguous and contradictory. The aim of this investigation is to study the anharmonic vibrational spectra of NAA, using density functional calculations. This molecule is of considerable importance from medical point of view. The understanding of vibrational spectrum might be helpful in understanding many medical processes.

2. Computational details

The density functional (DFT/B3LYP) at the 6-311+G(d,p) basis set level was adopted to calculate the properties of the title molecule in this work. All the calculations were performed using Gaussian 03W program package [8] with the default convergence criteria, without any constraint on the geometry [9]. The equilibrium geometry corresponding to the true minimum on the potential energy surface (PES) has been obtained by solving self-consistent field equation

* Corresponding author. Tel.: +91 9442068405.
E-mail address: sundaraganesan_n2003@yahoo.co.in (N. Sundaraganesan).

1386-1425/$ – see front matter © 2010 Elsevier B.V. All rights reserved.
doi:10.1016/j.saa.2010.06.034

Table 1a
Geometrical parameters optimized in naphthaleneacetic acid bond length (Å), bond angle (°) and dihedral angle (°).

Parameters	B3LYP/6-311+G(d,p)	XRD[a], naphthalene acetic acid	Parameters	B3LYP/6-311+G(d,p)	XRD[a], naphthalene acetic acid
Bond length (A°)			C5–C4–H13	118.77	119.5
C1–C2	1.372	1.365(3)	C4–C5–C6	119.44	119.03(16)
C1–C6	1.434	1.416(2)	C4–C5–C7	121.40	121.88(18)
C1–C18	1.512	1.500(2)	C6–C5–C7	119.17	119.08(19)
C2–C3	1.416	1.394(3)	C1–C6–C5	118.94	118.88(15)
C2–H11	1.086	0.930	C1–C6–C10	122.73	123.38(16)
C3–C4	1.373	1.336(3)	C5–C6–C10	118.33	117.74(16)
C3–H12	1.084	0.930	C5–C7–C8	120.96	121.2(2)
C4–C5	1.421	1.405(3)	C5–C7–H14	118.61	119.4
C4–H13	1.085	0.930	C8–C7–H14	120.43	1194
C5–C6	1.418	1.422(2)	C7–C8–C9	120.01	120.3(2)
C5–C7	1.422	1.406(3)	C7–C8–H15	120.23	119.8
C6–C10	1.422	1.413(2)	C9–C8–H15	119.76	119.8
C7–C8	1.372	1.341(4)	C8–C9–C10	120.56	121.0(2)
C7–H14	1.085	0.930	C8–C9–H16	119.68	119.5
C8–C9	1.416	1.386(4)	C10–C9–H16	119.76	119.5
C8–H15	1.084	0.930	C6–C10–C9	120.97	120.6(2)
C9–C10	1.372	1.360(3)	C6–C10–H17	119.84	119.7
C9–H16	1.084	0.930	C9–C10–H17	119.18	119.7
C10–H17	1.083	0.930	C1–C18–H19	109.16	108.6
C18–H19	1.095	0.970	C1–C18–H20	112.33	108.6
C18–H20	1.090	0.970	C1–C18–C21	115.45	114.62(13)
C18–C21	1.535	1.500(2)	H19–C18–H20	106.62	107.6
C21–O22	1.198	1.220(19)	H19–C18–C21	106.13	108.6
C21–O23	1.353	1.2759(19)	H20–C18–C21	106.64	108.6
O23–H24	0.968	0.93(3)	C18–C21–O22	123.40	122.59(15)
Bond angle (°)			C18–C21–O23	115.56	114.75(14)
C2–C1–C6	119.26	118.83(15)	O22–C21–O23	121.00	122.64(14)
C2–C2–C18	120.03	120.60(16)	C21–O23–H24	109.47	114.4(17)
C6–C1–C18	120.71	120.57(15)	*Dihedral angle* (°)		
C1–C2–C3	121.67	122.00(19)	C2–C1–C6–C10	179.30	−179.14(15)
C1–C2–CH11	119.27	119.0	C18–C1–C6–C5	179.94	178.64(12)
C3–C2–H11	119.04	119.9			
C2–C3–C4	120.01	120.17(19)			
C2–C3–H12	119.51	119.9			
C4–C3–CH12	120.48	119.9			
C3–C4–C5	120.67	121.07(17)			
C3–C4–CH13	120.56	119.5			
Dihedral angle (°)			C1–C2–C3–C4	0.24	−0.6(3)
C2–C1–C18–H19	13.40		C1–C2–C3–H12	179.72	
C2–C1–C18–H20	131.43		H11–C2–C3–C4	−178.67	
C2–C1–C18–C21	−106.01	−110.23(16)	C4–C5–C7–C8	179.57	−179.27(19)
C6–C1–C18–H19	−167.12		C1–C6–C10–C9	179.81	−179.13(17)
C6–C1–C18–H20	−49.09		C1–C18–C21–O22	−146.90	24.3(3)
C6–C1–C18–C21	73.47	69.8(2)	C1–C18–C21–O23	35.49	−157.00(17)

[a] Taken from Ref. [15].

effectively. The virbational spectra of the NAA have been obtained by taking the second derivative of energy, computed analytically. Multiple scaling of the force field has been performed by SQM procedure [10,11] to offset the systematic error caused by basis set incompleteness, neglect of electron correlation and vibrational anharmonicity [12]. The Potential Energy Distribution (PED) were carried out with the MOLVIB program written by Sundius [13,14]. Harmonic frequencies were calculated at DFT (B3LYP) level of theory. Vibrational frequencies computed at DFT level have reliable one-to-one correspondence to experimental IR and Raman frequencies [7]. Anharmonic calculations have been performed using the vibrational self-consistent field (VSCF) method which computes the vibrational frequencies including anharmonic effects. This type of calculation requires input from a previous harmonic vibrational computation. The wavenumbers obtained from the second-order perturbation theory (PT2) have been used in this investigation.

The natural bonding orbitals (NBO) calculations [15] were performed using NBO 3.1 program as implemented in the Gaussian 03W [8] package at the DFT/B3LYP/6-311+G(d,p) level in order to understand various second-order interactions between the filled orbitals of one subsystem and vacant orbitals of another subsystem, which is a measure of the intermolecular delocalization or hyper conjugation.

2.1. Molecular geometry

The crystal structure of the title NAA was originally determined by Rajan [16] using intensity data estimated from Weissenberg

Table 1b
Intermolecular hydrogen bonding parameters of NAA based on B3LYP/Aug-CC-PVDZ) method.

O23–H24···O46	O23–H24 0.951 Å (0.93)	H24–O46 2.222 Å (2.61)	O23···O46 3.234 Å (3.541(2))	O23–H24···O46 175.8° (177°)
O47–H48···O22	O47–H48 0.956 Å (0.93(3))	H48–O22 2.340 Å (2.87)	O47···O28 3.321 Å (3.746(2))	O47–H48···O22 173.2° (168(3))

Inside bracket experimental values.

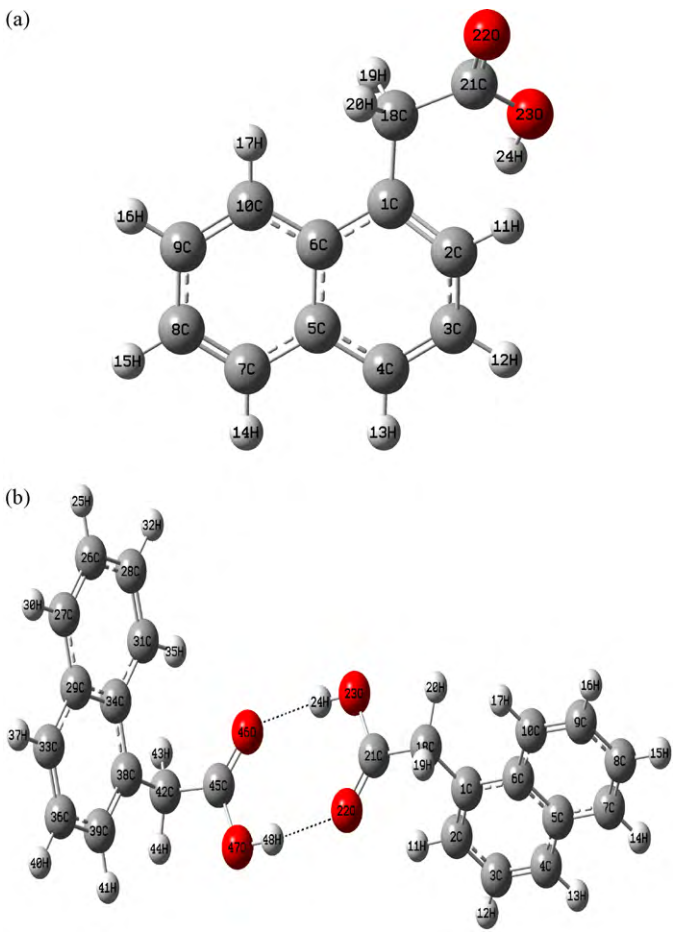

Fig. 1. (a) Molecular structure and atom numbering scheme adopted in this study for naphthalene acetic acid monomer and (b) dimer formation.

films. Li et al. [17] redetermination provides a structure with significantly improved precision with respect to the geometric parameters. In the crystal structure, intermolecular O–H···O hydrogen bonds, weak C–H···O hydrogen bonds and C–H_2 interactions link the molecules into a two-dimensional sheet lying parallel to (1 0 0). The structure is monoclinic of the space group $P2_1/c$, with $a = 12.7079(19)$, $b = 5.1464(8)$, $c = 15.014(2)$ Å, $Z = 4$. The optimized structure parameters and dimer parameters of NAA calculated by DFT (B3LYP) with the 6-311+G(d,p) and Aug-CC-PVDZ basis set show strong hydrogen bonding, which is listed in Tables 1a and 1b respectively, in accordance with the atom numbering scheme for a monomer (a) and dimer (b) given in Fig. 1a and b.

As there are three rotamers, viz., the around C1–C18, C18–C21 and C21–O22, the NAA molecule can exist in two forms: trans and cis. The minimum among all possible minima subjected to investigation has been identified through semi-empirical method. The total energy for cis form is equal to −613.89089 a.u. and for trans form is equal to −613.89299 a.u. by B3LYP/Aug-CC-PVDZ method. Of the two forms, the stable isomer is trans one since it possess lower energy when compared with cis form.

Optimized geometry shows that NAA molecular structure is not planar as it is evidence from O23–C21–C18–C1 and O22–C21–C18–C1 dihedral angles are 35.49° and −146.90° respectively. This is due to the consequence of steric repulsion between the hydrogen atom H24 with the oxygen atom. The calculated dihedral angles C2–C1–C6–C10 (179.30°), C9–C10–C6–C1 (179.81°), C3–C4–C5–C7 (−179.87°) and C8–C7–C5–C4 (179.57°) show that the naphthalene ring is coplanar.

Since, large deviation from experimental C–H bond lengths may arise from the low scattering factors of hydrogen atoms in the X-ray diffraction experiment, we did not include lack of C–H experimental bond length. This overestimation is also verified by in our calculation as represented in Table 1a. The experimental values of C–H bond lengths is ∼0.9300 Å [17] while the value in the theoretical results are bigger than ∼0.7 Å. The interaction of the carboxylic acid group on the naphthalene ring is of great importance in determining its structure and vibrational properties. It is observed that the influence of the substituent on the molecule play a vital role particularly in the C–C bond distance of the ring carbon atoms. As it is evident from the bond lengths of C1–C2 and C1–C6 (ring 1) is 1.372 and 1.434 Å, show slight deviation when compared with C6–C10 and C9–C10 of 1.422 and 1.372 Å (for ring 2), and symmetry of naphthalene ring is distorted, yielding ring angles smaller and larger than the normal value of 120° exactly at the substitution as shown in Table 1a. The C1–C2–C6 angle is 119.26° and C6–C10–C9 angle is 120.97° for ring 1 and 2.

The C_{acetic}–$C_{carboxylicacid}$ i.e. (C18–C21) bond length calculated by B3LYP/6-311+G(d,p) method is 1.535 Å is longer than that of X-ray data of similar molecule by 0.35 Å. The C21–O22 and O23–H24 bond length computed by B3LYP/6-311+G(d,p) method was 1.198 and 0.968 Å respectively. In international tables for crystallography [18] the C=O bond length in the carboxylic acid group confirming to the average value are tabulated for an aromatic carboxylic acid in which C=O is 1.266(20) Å and C–O is 1.305(20) Å. Our group also predicted the corresponding bond length in naphthoic acid are 1.218 and 1.362 Å by B3LYP method [6]. For the title molecule, the corresponding bond length are 1.220(19) and 1.275(19) [17], which are calculated as 1.198 and 1.353 Å by B3LYP method. Overall computed data by B3LYP/6-311+G(d,p) method show good agreement with X-ray data of NAA molecule [17].

From the theoretical values, it can be found that most of the optimized bond lengths are slightly higher than the experimental values. The largest deviations of bond lengths and bond angles between the theoretical values and experimental ones are 0.183 and 1.6 Å. The deviations can be attributed to the fact that the theoretical calculations were aimed at the isolated molecules in the gaseous phase and the experimental results were aimed at the molecule in the solid state. Despite these differences, the calculated geometrical parameters represents good approximation, and they are the basis for the calculations of other parameters such as vibrational frequencies and NBO analysis.

2.2. Hydrogen bonding

The structures shows the presence of intermolecular hydrogen bond interaction in NAA as shown in Fig. 1(b). In our present study the hydrogen bond analysis is carried out by B3LYP/Aug-CC-PVDZ method as shown in Table 1b. The strong hydrogen bond type of interaction between O23–H24···O46 and O47–H48···O22 is observed, the distance between O23···O46 and O47···O28 is about 3.234 and 3.321 Å respectively, are well within the range <3.0 Å for hydrogen interaction [19]. The other parameters i.e. the bond angles between the hydrogen bonding are also shown in Table 1b.

2.3. NBO analysis

NBO analysis provides the most accurate possible 'natural Lewis structure' picture of ϕ, because all orbital details are mathematically chosen to include the highest possible percentage of the electron density. A useful aspect of the NBO method is that it gives information about interactions in both filled and virtual orbital spaces that could enhance the analysis of intra- and intermolecular interactions.

Table 2a
Second-order perturbation theory analysis of Fock matrix in NBO basis for NAA.

Donor (i)	Type	ED/e	Acceptor (j)	Type	ED/e	$E^{(2)}$[a] (kJ/mol)	$E(j)-E(i)$[b] (a.u.)	$F(i,j)$[c] (a.u.)
C1–C2	σ	1.96610	C1–C6	σ*	0.029	5.53	1.26	0.074
			C1–C18	σ*	0.037	5.74	1.35	0.079
			C2–C3	σ*	0.016	3.17	1.25	0.056
			C6–C10	σ*	0.026	3.27	1.24	0.057
			C18–H19	σ*	0.038	6.80	0.72	0.067
			C18–H20	σ*	0.041	7.05	0.70	0.067
	π	1.68995	C3–C4	π*	0.270	19.06	0.28	0.066
			C5–C6	π*	0.485	18.86	0.29	0.069
C1–C6	σ	1.95437	C1–C2	σ*	0.029	4.79	1.25	0.069
			C1–C18	σ*	0.037	6.28	1.36	0.083
C1–C18	σ	1.93729	C18–H19	σ*	0.038	6.39	1.24	0.080
			C18–H20	σ*	0.041	6.23	1.22	0.078
			C18–C21	σ*	0.042	12.30	1.39	0.118
C3–C4	σ	1.97891	C2–C3	σ*	0.016	2.77	1.25	0.047
			C2–H11	σ*	0.013	2.15	1.29	0.047
	π	1.71829	C1–C2	π*	0.303	19.03	0.29	0.067
			C5–C6	π*	0.485	17.95	0.29	0.068
C5–C6	σ	1.96281	C1–C6	σ*	0.037	5.12	1.26	0.072
			C4–C5	σ*	0.024	4.39	1.25	0.066
			C5–C7	σ*	0.024	4.28	1.25	0.066
			C6–C10	σ*	0.026	4.46	1.25	0.067
	π	1.52249	C1–C2	π*	0.303	18.95	0.28	0.069
			C3–C4	π*	0.270	17.04	0.27	0.064
			C7–C8	π*	0.272	17.71	0.27	0.065
			C9–C10	π*	0.281	18.04	0.27	0.065
C7–C8	π	1.97929	C5–C6	π*	0.485	17.56	0.30	0.068
			C9–C10	π*	0.281	20.37	0.28	0.067
C9–C10	π	1.72466	C5–C6	π*	0.485	17.77	0.30	0.069
			C7–C8	π*	0.272	18.73	0.28	0.065
C18–H19	σ	1.92729	C21–O23	σ*	0.078	12.98	0.94	0.099
O22	LP(1)	1.98298	C21–O23	σ*	0.078	16.13	0.65	0.092
O23	LP(1)	1.97201	C18–C21	σ*	0.042	5.67	1.21	0.074
	LP(2)	1.80423	C21–O22	π*	0.160	17.22	0.59	0.091
C3–C4	π*	0.27012	C1–C2	π*	0.303	224.10	0.01	0.080
			C5–C6	π*	0.485	246.44	0.01	0.081
C7–C8	π*	0.27158	C5–C6	π*	0.485	195.63	0.02	0.082
C9–C10	π*	0.28139	C5–C6	π*	0.485	164.89	0.02	0.081
C21–O22	σ	0.11869	C21–O22	π*	0.160	710.20	0.02	0.266

[a] $E^{(2)}$ means energy of hyper conjugative interaction (stabilization energy).
[b] Energy difference between donor and acceptor i and j NBO orbitals.
[c] $F(i,j)$ is the Fock matrix element between i and j NBO orbitals.

The second-order Fock matrix was carried out to evaluate the donor–acceptor interactions in the NBO analysis [20]. The interactions result is a loss of occupancy from the localized NBO of the idealized Lewis structure into an empty non-Lewis orbital. For each donor (i) and acceptor (j), the stabilization energy $E(2)$ associated with the delocalization $i \rightarrow j$ is estimated as

$$E_2 = \Delta E_{ij} = q_i \frac{F(i,j)^2}{\varepsilon_j - \varepsilon_i}$$

where q_i is the donor orbital occupancy, ε_i and ε_j are diagonal elements and $F(i, j)$ is the off diagonal NBO Fock matrix element.

Natural bond orbital analysis provides an efficient method for studying intra- and intermolecular bonding and interaction among bonds, and also provides a convenient basis for investigating charge transfer or conjugative interaction in molecular systems. Some electron donor orbital, acceptor orbital and the interacting stabilization energy resulted from the second-order micro-disturbance theory are reported [21,22]. The larger the $E(2)$ value, the more intensive is the interaction between electron donors and electron acceptors, i.e. the more donating tendency from electron donors to electron acceptors and the greater the extent of conjugation of the whole system. Delocalization of electron density between occupied Lewis-type (bond or lone pair) NBO orbitals and formally unoccupied (antibond or Rydgberg) non-Lewis NBO orbitals correspond to a stabilizing donor–acceptor interaction. NBO analysis has been performed on the molecule at the DFT/B3LYP/6-311+G(d,p) level in order to elucidate the intramolecular, rehybridization and delocalization of electron density within the molecule. The intramolecular interaction are formed by the orbital overlap between σ(C–C) and σ*(C–C) and π(C–C) and π*(C–C) bond orbital which results intramolecular charge transfer (ICT) causing stabilization of the system. These interactions are observed as increase in electron density (ED) in C–C antibonding orbital that weakens the respective bonds. The electron density of conjugated bond of naphthalene ring (~1.97e) clearly demonstrate strong delocalization.

The strong intramolecular hyper conjugation interaction of the σ and π electrons of C–C, C–H and C–O to the anti C–C, C–H and C–O bond of the ring as well as acetic and acid group leads to stabilization of some part of the ring as evident from Table 2a. The intramolecular hyperconjugative interaction of the σ(C1–C2) distribute to σ*(C1–C8), (C1–C18), (C2–C3), (C6–C10), (C18–H19), (C18–H20) leading to stabilization of 5.0 kJ/mol. This enhanced further conjugate with antibonding orbital of π*(C3–C4) and (C5–C6) which leads to strong delocalization of 19.06 and 18.86 kJ/mol, respectively. The same kind of interaction is calculated in the C3–C4, C1–C18 and C5–C6 bond for NAA as shown in Table 2a. The most interaction energy, related to the resonance in the molecule, is electron donating from the LP(1)O22, LP(1)O23, LP(2)O23 to the anitbonding acceptor σ*(C21–O23), (C18–C21) and π*(C21–O22) of the acid group leads to moderate stabilization energy of ~15 kJ/mol is shown in Table 2a. The π*(C7–C8) and (C9–C10) of the NBO conjugated with π*(C5–C6) resulting to an enormous stabilization of

Table 2b
Second-order perturbation energies $E^{(2)}$ (donor → acceptor) for NAA.

Donor (i)	Acceptor (j)	$E^{(2)}$[a] (kJ/mol)	$E(j)-E(i)$[b] (a.u.)	$F(i,j)$[c] (a.u.)
Within unit 1				
LP(1)O22	σ*(C18–C21)	4.83	0.65	0.05
LP(1)O22	σ*(C21–O22)	10.88	0.74	0.08
LP(1)O23	π*(C21–O22)	69.28	0.28	0.12
From unit 1 to unit 2				
LP(1)O22	σ*(O47–H48)	4.34	0.96	0.05
LP(1)O22	σ*(O47–H48)	106.02	1.27	0.32
LP(1)O23	π*(C45–O46)	0.07	0.89	0.007
LP(2)O23	π*(C45–O46)	0.22	0.35	0.008
From unit 2 to unit 1				
LP(1)O46	σ*(O23–H24)	12.15	0.95	0.09
LP(2)O46	σ*(O23–H24)	56.49	1.11	0.22
LP(2)O47	σ*(C21–O22)	0.20	0.36	0.01
LP(2)O47	σ*(C21–O22)	0.06	0.52	0.07
Within unit 2				
LP(2)O46	σ*(C42–C45)	14.76	0.90	0.10
LP(2)O46	σ*(C45–O47)	6.29	1.02	0.07
LP(2)O47	π*(C45–O46)	28.85	0.43	0.10
LP(2)O47	σ*(O47–H48)	25.71	1.02	0.14

[a] $E^{(2)}$ means energy of hyper conjugative interaction (stabilization energy).
[b] Energy difference between donor and acceptor i and j NBO orbitals.
[c] $F(i,j)$ is the Fock matrix element between i and j NBO orbitals.

195.63 and 164.89 kJ/mol respectively. The another interaction is calculated at σ(C21–O22) with π*(C21–O22) shows enormous stabilization energy of 710.20 kJ/mol.

The importance of hyper conjugation and electron density transfer from lone electron pairs of the Y atom to the X–H antibonding orbital in the X–H···Y system has been reported [23]. The intermolecular O–H···O hydrogen bonding is formed by the orbital overlap between the n(O) and σ*(O–H) which results intramolecular charge transfer (ICT) causing stabilization of the H-bonded systems. Hence hydrogen bonding interaction leads to an increase in electron (ED) of O–H antibonding orbital. The increase of the population of C–O antibonding orbital weakens the C–O bond.

Thus the nature and strength of the intermolecular hydrogen bonding can be explored by studying the changes in electron density in the vicinity of O···H hydrogen bonds. The NBO analysis of NAA clearly explains the evidences of the formation of strong H-bonded interaction between the LP(O) and σ*(O–H) antibonding orbitals. The stabilization energy $E^{(2)}$ associated with hyperconjugative interaction n_1 (O22) → σ*(O47–H48), n_1 (O22) → σ*(O47–H48) and n_1 (O46) → σ*O23–H24 and n_2 (O46) → σ*O23–H24 are obtained as 4.34, 106.02 and 12.15, 56.49 kJ/mol respectively are shown in Table 2b which quantify the extend of intermolecular hydrogen bonding. The differences in $E^{(2)}$ energies are reasonably due to fact that the accrual of electron density in the O–H bond is not only drawn from the n(O) of hydrogen-acceptor but also from the whole molecule.

2.4. Vibrational spectral analysis

The naphthaleneacetic acid molecule shows C_s point group symmetry. Its 66 modes of vibration can accordingly be classified into the irreducible representation 45A′ + 21A″. Not much attempt has been made in the past to provide a detailed and a complete assignment to the vibrational modes. While Krishnakumar et al. [7] presumed a C_s point group structure for the molecule and provided assignments to some of the more intense vibrational bands using harmonic vibrational frequencies. The present work deals with complete vibrational analysis on the basis of DFT calculated anharmonic frequencies. The results of B3LYP/6-311+G(d,p) calculations are given in Table 3 and compared with experimental data.

2.4.1. C–H vibrations

The hetero aromatic structure shows the presence of C–H stretching vibration in the region 3100–3000 cm^{-1} which is the characteristic region for the ready identification of C–H stretching vibration [24,25]. In this region the bands are not affected appreciably by the nature of substituent. Two benzene rings are fused together in NAA molecule, it has seven adjacent C–H moieties. The expected seven C–H stretching vibrations corresponding to stretching modes of C2–H, C3–H, C4–H, C7–H, C8–H, C9–H and C10–H units. The weak bands in FT-IR at 3068, 3054, 3066 cm^{-1} as a strong band and 3051 cm^{-1} in FT-Raman spectrum is assigned to C–H stretching vibration. The anharmonic vibrations (mode nos. 2–8) by B3LYP/6-311+G(d,p) method predict at 3065, 3058, 3033, 3020, 3010, 3001 and 3000 cm^{-1} fall within the recorded spectral range. As expected these modes are pure stretching modes as it is evident from PED column, they are exactly contributing to 99%.

The in-plane aromatic C–H bending vibration occurs in the region 1400–1000 cm^{-1}, the bands are sharp but are weak to medium intensity. The C–H in-plane-bending anharmonic vibrations computed at 1424, 1394, 1265, 1232, 1187, 1178, 1153 and 1045 cm^{-1} (mode nos. 18–19, 24–25, 27–30 and 33) by B3LYP method show excellent agreement with medium FT-IR band at 1410, 1265, 1252 cm^{-1} and 1275, 1232, 1189, 1171 cm^{-1} in FT-Raman spectrum. The PED corresponds to this mode is a mixed mode as it is evident from Table 3.

The band observed at 1010, 979, 931, 878, 800 cm^{-1} in FT-IR and 1018, 979, 949 and 876 cm^{-1} in FT-Raman spectrum are assigned to C–H out-of-plane bending vibrations for NAA. This also shows good agreement with theoretical anharmonic wavenumber values at 1025–804 cm^{-1} (mode nos. 34–40 and 41) by B3LYP method. The PED also show mixed contribution of approximately 80% for these vibrations.

2.4.2. Methylene group vibrations

For the assignments of CH_2 group frequencies, basically six fundamentals can be associated to each CH_2 group namely, CH_2 sym, symmetric stretch, CH_2 asym, asymmetric stretch, CH_2 scis, scissoring and CH_2 rock, rocking modes which belong to polarized in-plane vibrations of A′ species. In addition to that CH_2 wag, wagging and CH_2 twist, twisting modes of CH_2 group would be expected to be depolarized for out-of-plane bending vibrations.

Table 3
Vibrational wavenumbers obtained for NAA at B3LYP/6-311+G(d,p) method [harmonic and anharmonic (cm^{-1}), IR_{int} ($K\,mmol^{-1}$)].

Mode nos.	Species	Experimental[a] (cm^{-1})		Theoretical wavenumber (cm^{-1})		(PED ≥ 10%)
		FT-IR	FT-Raman	Harmonic[a]	Anharmonic	
1	A′	3425w		3433	3534	OH str(100)
2	A″		3073w	3083	3065	CH str(99)
3	A′	3068w	3066s	3066	3058	CH str(99)
4	A′	3054w	3051w	3040	3033	CH str(99)
5	A′			3019	3020	CH str(99)
6	A′			2968	3010	CH str(99)
7	A′	3012w	3013w	2934	3001	CH str(99)
8	A′	3003w		2922	3000	CH str(99)
9	A′		2949w	3004	2948	C–H in CH_2 str(50), CH2asy str(43)
10	A′	2912w		2946	2918	C–H in CH_2 str(57), CH2sym str(43)
11	A′	1696vs	1674w	1667	1723	C═O str(84)
12	A′	1631w	1624w	1654	1622	C–C str(64), C–H ipb(18)
13	A′	1597m	1602w	1635	1602	C–C str(66), C–H ipb(26)
14	A′		1584vs	1591	1579	C–C str(69), C–H ipb(14)
15	A′	1509s		1552	1513	C–C str(52), C–H ipb(40)
16	A′			1536	1467	C–H ipb(57), C–C str(36)
17	A′		1447ms	1518	1435	CH_2 sci(95)
18	A′	1410s	1410w	1508	1424	C–H ipb(56), C–C str(30)
19	A′			1480	1394	C–H ipb(64), C–C str(22)
20	A′	1385w	1362vs	1455	1364	C–C str(25), CH_2 wag(19), C–O ipb(11),
21	A′	1346m		1405	1351	C–C str(59), C–O ipb(12),
22	A′	1291w		1383	1279	C–C str(34), C–O ipb(14), C–H ipb(13)
23	A′		1339w	1366	1287	CH_2 wag(29), C–H ipb(21), C–C str(21), C–CH_2 str(12)
24	A′	1265m	1275vw	1357	1265	C–H ipb(38), C–C str(25), Ring 1 tridef(15)
25	A′	1252ms	1232w	1335	1232	C–H ipb(33), C–C str(25), Ring 1 tridef(13)
26	A′	1218vs	1214w	1321	1216	CH_2 twi(34), C–H ipb(20), C–C str(11)
27	A′		1189w	1298	1187	C–H ipb(48), C–C str(16), CH_2 twi(34)
28	A′		1171w	1297	1178	C–H ipb(79), C–C str(17)
29	A′	1163w		1256	1173	CH_2 twi(29), C–O ipb(16), C–O str(16)
30	A′		1151w	1236	1153	C–H ipb(43), C–C str(30), Ring 1 tridef(15)
31	A′	1135w		1219	1136	C–C str(60), C–H ipb(24), CH_2 twi(10)
32	A′	1073w	1081s	1193	1078	C–C str(68), C–H ipb(11),
33	A′		1055w	1168	1045	C–H ipb(25), Ring 1 tridef(19), C–C str(17)
34	A″	1010w	1018m	1163	1025	C–H opb(77), Ring 2 tridef(10)
35	A′			1149	985	C–H opb(84)
36	A′	979w	979vw	1130	978	C–H opb(89)
37	A′		949w	1121	958	C–H opb(80), C–C str(18)
38	A″	931ms		1084	919	C–H opb(39), CH_2 rock(24)
39	A″			1072	912	C–H opb(64), CH_2 rock(18)
40	A′	878w	876w	1060	879	C–H opb(76),Ring 1 puck(10)
41	A′	856w	853w	1040	870	C–COOH str(27), C–O str(23), CH_2 rock(20)
42	A″		828w	1024	837	C–COOH opb(81), C–H opb(10)
43	A″	800m		1007	804	C–H opb(21), Ring 1 tridef(13), C–CH_2 str(12), Ring 2 tridef(10)
44	A″			968	794	Ring 1 puck(25), C–H ipb(18)
45	A″	780vs	775w	952	783	C–C str(18), Ring 1 tridef(16), Ring 2 tridef(12)
46	A″	754w	742w	937	741	Ring 2 puck(19), C–C str(17), C–O opb(16), Ring 1 puck(10)
47	A″			851	733	C–H opb(84)
48	A″	690m	692s	830	675	C–O opb(19),C–H opb(17)
49	A′	624ms		781	629	Ring 2 puck(28), Ring 1 puck(26), t Ring 1(19), C–H opb(12)
50	A′		607w	746	607	C–O opb(44), C–CH_2 opb(41),
51	A″		564w	732	581	Ring 2 puck(28), Ring 1 puck(26), t Ring 1(19), C–H opb(12)
52	A′	536s	539m	688	540	t Ring 1(30), C–H opb(20), t Ring 1(16), C–CH_2 opb(16), t Ring 2(11)
53	A′			675	527	Ring 2 asy def(38), C–H opb(12),CCC obp(11)
54	A′	516w	514vs	643	517	Ring 1 asy def(31), C–C str(25)
55	A′	502w	502ms	622	490	t Ring 2(36), t Ring 1(22)
56	A″		488w	602	473	wag C–C(68)
57	A″		429w	570	428	wag C–O(58) CCC ipb(20)
58	A″	412w	416w	555	419	wag C–O(58) CCC ipb(18)
59	A″		355w	541	358	C–COOH ipb(54), CCC ipb(10)
60	A″		290w	502	278	CH_2 (twisting) (61)
61	A″		257w	489	260	tRsym(56)
62	A″		180w	455	174	C–COOH opb(48), CCC opb(18)
63	A″			358	148	tRsym(56)tRtrig(20)
64	A″			298	72	tRaym(55)tRtrig(20)
65	A″			256	37	tRasym(56)tRsym(20)
66	A″			180	53	Butterfly(71)

Abbreviations used R: ring; ss: symmetric stretching; b: bending; d: deformation; asy: asymmetric; waging; t: torsion; trig: trigonal; υ: stretching, ipb-in-plane bending, opb-out-of-plane bending.

[a] Taken from Ref. [7].

The C–H stretching vibrations of the methylene group is at lower frequencies than those of the aromatic C–H ring stretching. The asymmetric CH_2 stretching vibration generally observed in the region 3000–2900 cm^{-1}, while the CH_2 symmetric stretch will appear between 2900 and 2800 cm^{-1} [26,27]. The CH_2 asymmetric and symmetric stretching vibrations are observed in FT-IR and FT-Raman spectrum as a weak intensity bands as seen in Table 3 for our title molecule. The band 2949 cm^{-1} in FT-Raman spectrum and the band at 2912 cm^{-1} in FT-IR are assigned to CH_2 asymmetric and symmetric stretching vibration. However, in view of our results, the assignment of CH_2 asymmetric stretching band, suggested in Ref. [7] should be corrected (The FT-Raman band at 3073 cm^{-1} was assigned to a asymmetric stretching of CH_2). The theoretically computed anharmonic wavenumbers by B3LYP/6-311+G(d,p) method at 2948 and 2918 cm^{-1}(mode nos. 9 and 10) are assigned to CH_2 asymmetric and symmetric stretching vibrations for $C18H_2$ unit as shown in Table 3. The PED corresponding to both (asymmetric and symmetric) type of vibrations show as a pure mode of 98% as it is evident from Table 3.

In the present assignment the CH_2 bending modes follow, in decreasing wavenumber, the general order CH_2 deformation > CH_2 wagging > CH_2 twist > CH_2 rock. Since the bending modes involving hydrogen atom attached to the central carbon falls into the 1450–875 cm^{-1} range, there is extensive vibrational coupling of these modes with CH_2 deformations particularly with the CH_2 twist. It is notable that both CH_2 scissoring and CH_2 rocking modes were sensitive to the molecular confirmation. For cyclohexane, the CH_2 scissoring mode has been assigned to the medium intensity IR band at about 1450 cm^{-1} was assigned to CH_2 scissoring mode [28]. In our title molecule the anharmonic frequency computed by B3LYP/6-311+G(d,p) method at 1435 cm^{-1} (mode no. 17) is assigned to CH_2 scissoring. The calculated PED corresponding to this mode show that this mode is a pure mode with 95%.

The CH_2 wagging vibrations computed by B3LYP/6-311+G(d,p) method at 1364 cm^{-1}(mode no. 20). The PED corresponding to this modes is only 20%. The CH_2 twisting vibrations are observed as a weak band in FT-Raman spectrum at 1189 cm^{-1}. The PED analysis identifies the CH_2 twisting vibration combined with C–H in-plane bending and C–C stretching vibrations as evident from Table 3. The PED corresponding to this mode is 34%. The computed anharmonic wavenumber for this mode falls within the range of 1187 cm^{-1}(mode no. 27). The CH_2 rocking vibrations computed by B3LYP method show good agreement with experimental observations. The PED corresponds to the CH_2 rocking vibration is ~20% (mode nos. 38–39).

2.4.3. COOH vibrations

Carboxylic acid dimer is formed by strong hydrogen bonding in the solid and liquid state. Vibrational analysis of carboxylic acid group is made on the basis of carbonyl group and hydroxyl group. The C=O stretch of carboxylic acids is identical to the C=O stretch in ketones, which is expected in the region 1740–1660 cm^{-1} [29]. The C=O bond formed by P_π–P_π between C and O, internal hydrogen bonding reduces the frequencies of the C=O stretching absorption to a greater degree than does intermolecular H bonding because of the different electro-negativities of C and O, the bonding are not equally distributed between the two atoms. The lone pair of electrons on oxygen also determines the nature of the carbonyl groups. In our present study a very strong band observed in FT-IR spectrum at 1696 cm^{-1} is assigned to C=O stretching vibrations show moderate agreement with B3LYP value at 1723 cm^{-1} (mode no. 11). The B3LYP predicted value show a small deviation of about ~27 cm^{-1} with FT-IR data. But the PED corresponds to this vibration is 84%. The harmonic wavenumber predicted at 1667 cm^{-1} show excellent agreement with experimental data.

The free hydroxyl group absorbs strongly in the region 3700–3584 cm^{-1}, whereas the existence of intermolecular hydrogen bond formation can lower the O–H stretching frequency in the range 3500–3200 cm^{-1} with increase in intensity and breadth [30,31]. In the hydrogen-bonded dimer, the O–H stretching band of the COOH group in the IR spectrum centers around 3000 cm^{-1} and it is superimposed on the C–H stretching bands [32]. In our earlier study of ferulic acid [33] in the condensed state is characterized by a strongly bonded O–H group (O–H···O = 2.09 Å) with a broad O–H stretching band near 3000 cm^{-1}, which is superimposed on the C–H stretching bands. The broad wings of the O–H stretching band can be seen on either side of the C–H bands. The stretching vibrational wavenumber of free O–H is practically unchanged, while that of the bound O–H is red shifted. The red shift of the O–H stretching wavenumber is due to the formation of strong O–H···O hydrogen bonds by hyperconjucation between carbonyl oxygen lone electron pairs and σ^*O–H antibonding orbitals. This is due to the increase of electron density occurring at σ^*C=O and the antibonding orbitals π^* and the σ^*O–H. Consequently, these bonds become weaker and are elongated, and the respective stretching vibrational wavenumbers are red shifted [34]. Similarly in our case also the theoretical calculations of monomer predict the anharmonic wavenumber at 3534 cm^{-1} (mode no. 1) by B3LYP method is assigned to O–H stretching vibration, however the recorded FT-IR broad band at 3425 cm^{-1} show deviation about ~100 cm^{-1} is assigned to O–H stretching vibration this may be due to presence of strong hydrogen bonding in the COOH group. The present assignment agree very well with the values available in literature [35–37], the PED corresponds to this vibrations is exactly pure one contributing to 100%. The C–COOH in-plane and out-of-plane bending vibration computed value is in good agreement with experimental observations.

2.4.4. C–C vibrations

Naphthalene ring stretching vibrations are expected in the region 1620–1390 cm^{-1}. Naphthalene ring vibrations are found to make a major contribution in the IR and Raman spectra [38,39], the frequency observed in FT-IR spectrum at 1631, 1597, 1385, 1346, 1291 cm^{-1} and 1624, 1602, 1584, 1362 cm^{-1} have been assigned to C–C stretching vibrations. The theoretically predicted anharmonic frequencies at 1622–1279 cm^{-1}(mode nos. 12–14 and 20–22) by B3LYP/6-311+G(d,p) method show excellent agreement with experimental data. These vibrations are mixed up with C–H in-plane-bending vibrations as shown in Table 3. The PED corresponds to this vibrations is a mixed modes as evident from Table 3.

2.4.5. C–COOH vibrations

In p-chlorobenzoic acid, the band at 1175 cm^{-1} in FT-IR gas phase spectrum and medium absorption band at 1186 cm^{-1} in FT-Raman spectrum corresponds to C–COOH stretching vibration [40]. In our previous study of naphthoic acid [6], the band predicted at 1189 cm^{-1} by B3LYP method was assigned to C–COOH stretching vibration which is coupled with C–H in-plane-bending vibrations. In our present study the anharmonic frequency predicted at 870 cm^{-1} by B3LYP/6-311+G(d,p) method is assigned to C–COOH stretching vibration which is in exact correlation with recorded FT-IR value at 856 cm^{-1} (mode no. 41). The predicted value of 870 cm^{-1} show deviation ~299 cm^{-1} from literature value may be due to mixing of this vibration with CH_2 rocking vibration. The vibrational mode nos. 59 and 62 by B3LYP method at 358 and 174 cm^{-1} are assigned to C–COOH in-plane bending and out-of-plane bending vibrations show good agreement with recorded FT-Raman spectral data at 355 and 180 cm^{-1} respectively as well as literature data [41]. The PED of these modes are mixed one as it is shown in Table 3.

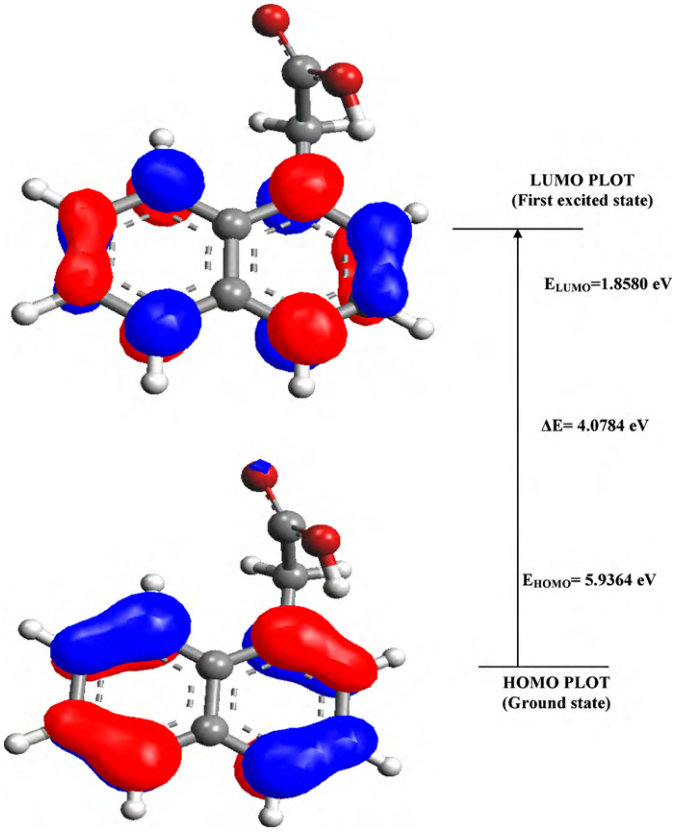

Fig. 2. The atomic orbital compositions of the frontier molecular orbital for NAA.

2.5. HOMO, LUMO analysis

Both the highest occupied molecular orbital (HOMO) and lowest unoccupied molecular orbital (LUMO) are the main orbital take part in chemical stability [41]. The HOMO represents the ability to donate an electron, LUMO as an electron acceptor represents the ability to obtain an electron. The HOMO and LUMO energy calculated by B3LYP/6-311+G(d,p) method as shown below. This electronic absorption corresponds to the transition from the ground to the first excited state and is mainly described by one electron excitation from the highest occupied molecular orbital (HOMO) to the lowest unoccupied molecular orbital (LUMO).

The HOMO is located over the acid group, the HOMO → LUMO transition implies an electron density transfer to ring from acid group. Moreover, these orbital significantly overlap in their position for NAA. The atomic orbital compositions of the frontier molecular orbital are sketched in Fig. 2.

HOMO energy (B3LYP) = 5.9364 eV

LUMO energy (B3LYP) = 1.8580 eV

HOMO–LUMO energy gap (B3LYP) = 4.0784 eV

The calculated self-consistent field (SCF) energy of NAA is −631.927448 a.u. The HOMO and LUMO energy gap explains the eventual charge transfer interactions taking place within the molecule.

3. Conclusions

Anharmonic vibrational analysis has been made in the present work for proper frequency assignments for naphthalene acetic acid. The equilibrium geometries of NAA have been determined and compared with X-ray crystal data. Anharmonic frequencies of NAA were determined and analyzed by DFT level of theory utilizing 6-311+G(d,p) basis set. Good agreement between the calculated and experimental spectra was obtained. The DFT/B3LYP/6-311+G(d,p) spectrum showed better agreement with experimental spectrum. However, the difference between the observed and scaled wavenumber values of O–H fundamental is very large, due to the fact that the presence of the intermolecular hydrogen bonds. The detailed anharmonic frequencies assignment of NAA, presented in this work has clarified several ambiguities in the previously reported investigation of the experimental spectra. NBO result reflects the charge transfer mainly due to O–H and N–H group.

References

[1] A. Goodman, Gilman (Ed.), Las Bases Famacolo's gicas de la Terapeutical, vol. II, ninth ed., Mc Graw Hill, Intermedicana, Me'jica, 1996.
[2] G.M. Chaban, J.O. Jung, R.B. Gerber, J. Chem. Phys. 111 (1999) 1823.
[3] A. Miani, E. Cane, P. Palmieri, A. Trombetti, J. Chem. Phys. 112 (2000) 248.
[4] K.V. Berezin, V.V. Nechaev, P.M. Elkin, Opt. Spectrosc. 97 (2004) 210.
[5] V. Krishnakumar, R. Mathammal, S. Muthunatesan, Spectrochim. Acta 70A (2008) 201.
[6] S. Chandra, H. Saleem, N. Sundaragnaesan, S. Sebastian, Spectrochim. Acta A 74 (2009) 704.
[7] V. Krishnakumar, R. Mathammal, S. Muthunatesan, Spectrochim. Acta 70A (2008) 210.
[8] Gaussian 03 Program, Gaussian Inc., Wallingford, CT, 2004.
[9] H.B. Schlegel, J. Comput. Chem. 3 (1982) 214.
[10] P. Pulay, G. Forgarasi, G. Pongor, J.E. Boggs, A. Vargha, J. Am. Chem. Soc. 105 (1983) 7073.
[11] G. Rauhut, P. Pulay, J. Phys. Chem. 99 (1995) 3093.
[12] J.B. Foresman, A. Frisch, Exploring Chemistry with Electronic Structure Methods, 2nd ed., Gaussian, Inc, Pittsburgh, PA, 1996.
[13] T. Sundius, MOLVIB: A Program for Harmonic Force Field Calculations, QCPE Program. No.604, J. Mol. Struct. 218 (1990) 321.
[14] T. Sundius, Vib. Spectrosc. 29 (2002) 89.
[15] E.D. Glendening, A.E. Reed, J.E. Carpenter, F. Weinhold, NBO version 3.1, TCI, University of Wisconsin, Madison, 1998.
[16] S.S.S. Rajan, Acta Cryst. 34B (1978) 998.
[17] Z.-A. Li, D.Y. Chen, L.-J. Liu, Acta Cryst. E 64 (2008) 2310.
[18] F.H. Allen, Acta Crystallogr. B 58 (2002) 380.
[19] G.A. Jaffrey, An Introduction to Hydrogen Bonding, Oxford University Press, 1997.
[20] M. Szafran, A. Komasa, E.B. Adamska, J. Mol. Struct. (Theochem.) 827 (2007) 101.
[21] C. James, A. Amal Raj, R. Reghunathan, I.H. Joe, V.S. Jayakumar, J. Raman Spectrosc. 37 (2006) 1381.
[22] J.N. Liu, Z.R. Chen, S.F. Yuan, J. Zhejiang Univ. Sci. B6 (2005) 584.
[23] J. Chocholousova, V.V. Spirko, P. Hobza, Phys. Chem. Chem. Phys. 6 (2004) 37.
[24] V.K. Rastogi, M.A. Palafox, R.P. Tanwar, L. Mittal, Spectrochim. Acta A 58 (2002) 1989.
[25] M. Silverstein, G. Clayton Basseler, C. Morill, Spectrometric Identification of Organic Compounds, Wiley, New York, 1981.
[26] D. Sajan, J. Binoy, B. Pradeep, K.V. Krishnan, V.B. Kartha, I.H. Joe, V.S. Jayakumar, Spectrochim. Acta A 60 (2004) 173.
[27] K. Furic, V. Mohack, M. Bonifacic, I. Stefanic, J. Mol. Struct. 267 (1992) 39.
[28] K.B. Wiberg, A. Sharke, Spectrochim. Acta A 29 (1973) 583.
[29] D.L. Vein, N.B. Colthup, W.G. Fateley, J.G. Grasselli, The Handbook of Infrared and Raman Characteristic Frequencies of Organic Molecules, Academic Press, San Diego, 1991.
[30] B. Smith, Infrared Spectral Interpretation, A Systematic Approach, CRC Press, Washington, DC, 1999.
[31] R.M. Silverstein, F.X. Webster, Spectroscopic Identification of Organic Compounds, sixth ed., John Wiley & Sons Inc., New York, 2003.
[32] N.B. Colthup, L.H. Daly, S.E. Wiberly, Introduction to Infrared and Raman Spectroscopy, Academic Press, New York, 1990.
[33] S. Sebastian, N. Sundaganesan, S. Manoharan, Spectrochim. Acta A 74 (2009) 312.
[34] J. Chocholousova, V. Spirko, P. Hobza, Phys. Chem. Chem. Phys. 6 (2004) 37.
[35] N. Sundaraganesan, B. Dominc Johsua, C. Meganathan, R. Meenashi, J.P. Cornard, Spectrochim. Acta A 70 (2008) 376.
[36] P. Venkoji, Ind. J. Pure Appl. Phys. 24 (1986) 567.
[37] J. Marshal, Ind. J. Phys. B 72 (1998) 661.
[38] C. Surisseau, P. Marvel, J. Raman Spectrosc. 25 (1994) 447.
[39] A.J. Barnes, M.A. Majid, M.A. Stuckey, P. Gregory, C.V. Stead, Spectrochim. Acta A 41 (1985) 629.
[40] N. Sundaragnesan, B. Anand, C. Meganathan, B.D. Joshua, Spectrochim. Acta A 69 (2008) 871.
[41] S. Gunasekaran, R.A. Balaji, S. Kumeresan, G. Anand, S. Srinivasan, Can. J. Anal. Sci. Spectrosc. 53 (2008) 149.